IOP Publishing Journal of Physics D: Applied Physics

J. Phys. D: Appl. Phys. **41** (2008) 115506 (13pp) doi:10.1088/0022-3727/41/11/115506

A simple formula for the effective complex conductivity of periodic fibrous composites with interfacial impedance and applications to biological tissues

Paolo Bisegna and Federica Caselli

Department of Civil Engineering, University of Rome 'Tor Vergata', 00133 Rome, Italy

E-mail: bisegna@uniroma2.it and caselli@ing.uniroma2.it

Received 11 February 2008, in final form 26 March 2008
Published 9 May 2008
Online at stacks.iop.org/JPhysD/41/115506

Abstract

This paper presents a simple analytical expression for the effective complex conductivity of a periodic hexagonal arrangement of conductive circular cylinders embedded in a conductive matrix, with interfaces exhibiting a capacitive impedance. This composite material may be regarded as an idealized model of a biological tissue comprising tubular cells, such as skeletal muscle. The asymptotic homogenization method is adopted, and the corresponding local problem is solved by resorting to Weierstrass elliptic functions. The effectiveness of the present analytical result is proved by convergence analysis and comparison with finite-element solutions and existing models.

(Some figures in this article are in colour only in the electronic version)

1. Introduction

This work presents a mathematical model of a biological tissue comprising tubular cells, such as skeletal muscle, and is aimed at determining the relationships between its effective dielectric properties and the properties of the constituent phases. This issue may be of significance to many applications for noninvasive diagnosis and treatment, such as electrical impedance tomography [1, 2], body composition [3], dialysis [4], radio-frequency hyperthermia and ablation [5].

The dielectric properties of tissues vary as a function of frequency: experiments show indeed three dispersions, α, β and γ, mainly attributed to different relaxation processes: ionic diffusion, interfacial polarization and dipolar orientation, respectively [6]. The β dispersion, considered herein, takes place in the radio-frequency range and principally arises from the capacitive charging of cellular membranes, known as the Maxwell–Wagner effect.

Different phenomenological relaxation models are available in the literature, ranging from the one-pole Debye model [7] to the famous Cole–Cole model [8], to recent parametric models [9, 10]. Equivalent-circuit models can also be found (e.g. [11–13]), but they pose the problem of parameter identification [14, 15].

Micromechanical approaches allow one to derive the effective (or equivalent) dielectric properties of the tissue from the properties of the constituent phases and to take into account microstructural details. Numerical solutions of the corresponding homogenization problems, based on finite element [16], boundary element [17], finite difference [18, 19] or transport lattice [20] methods are suitable, though in general computationally expensive. Analytical solutions [21, 22] have been obtained by introducing simplifying assumptions (e.g. dilute or differential schemes [23]), leading to closed-form results. Exact analytical solutions are more involved, and different mathematical methods have been developed to address the associate boundary value problems, characterized by partial differential equations with rapidly oscillating coefficients arising from the description of the microstructure.

In this work, the problem of the electrical conduction in a tissue comprising aligned tubular cells is studied, and the effective complex conductivity in the plane orthogonal to the fibres is obtained. An idealized model of the tissue is considered, composed of a periodic hexagonal arrangement of conductive circular cylinders embedded in a conductive matrix, with interfaces exhibiting a capacitive impedance, taking into account the dielectric behaviour of cell membranes. A rigorous, analytical solution to the homogenization problem is provided by employing the asymptotic homogenization method [24, 25], whose central step is the solution of the so-called cell (or local) problem (equations (17)–(19)). In most cases, numerical techniques are needed; here, it is solved in closed form, making use of Weierstrass elliptic functions [26–28].

A related approach was followed by other authors to compute the effective elastic properties of composite materials with a regular structure [29, 30]. Other relevant citations are: [31, 32], based on the Rayleigh identity and devoted to effective transport properties of a regular array of cylinders; [33], dealing with a doubly periodic parallelogrammic array of elastic cylindrical inclusions embedded in an elastic matrix; [34], studying the effective response of a periodic fibre reinforced material to SH wave propagation.

In the cited literature, the unknown fields were continuous across the interfaces. This is not the case in this work, dealing with interfaces exhibiting a capacitive impedance, which causes a jump in the electric potential. Related problems were treated in [35, 36], involving interfaces with an inherent electric or thermal resistance, and in [37, 38], dealing with interfaces having a lumped elastic compliance. Particularly relevant to the present work is [35], where a closed-form formula for the effective thermal conductivity of a square array of cylindrical inclusions was derived.

The following solution strategy is adopted here. The unknown is represented, in the fibres and in the matrix, as the real part of an analytic function (equations (23) and (24)), thus satisfying the harmonic field equation. Then, the interface conditions are exploited in order to link the fibre and matrix expressions. Finally, the solution in the matrix is represented by resorting to Weierstrass elliptic functions in order to account for the periodicity conditions (equation (30)). The solution of the cell problem results from the identification of the two series representations in the matrix. This approach leads to a simple closed-form formula for the effective complex conductivity in the plane orthogonal to the fibres (equation (43)), which, to the authors' knowledge, is new in the literature.

This formula has been validated by using finite-element solutions as a benchmark and a complete agreement has been obtained. A comparison with the well-known Pauly–Schwan (PS) and Hanai–Asami–Koizumi (HAK) models of the effective complex conductivity of cell suspensions is also presented. Moreover, the number of relaxation processes accounted for by the present theory is discussed, and their relative importance is investigated. Eventually, a parametric analysis is performed, emphasizing the influence of microstructural parameters on the conductivity locus and the membrane potential.

The homogenization problem solved herein is formally analogous, e.g. to the electric or thermic conduction problem of a periodic fibrous composite with interfacial resistance, or to the antiplane shear problem of a periodic fibrous composite with elastic constituents and Kelvin–Voigt viscoelastic interfaces. Hence, the analytical formula derived herein may also be used to compute the corresponding effective electrical, thermal or mechanical properties.

The paper is organized as follows. In section 2 the statement of the problem is given and the asymptotic homogenization method is sketched. The main result is presented in section 3, where the cell problem is analytically solved, and the closed-form formula (43) for the effective complex conductivity is provided. Section 4 is devoted to validation, comparison, discussion and parametric analysis. Results from the elliptic function theory used in section 3 are collected in appendix A; a result from linear algebra used in section 3.5 is recalled in appendix B.

2. Statement of the problem

A two-phase fibrous composite material composed of a periodic hexagonal arrangement of identical circular cylinders with radius R and electric conductivity σ_{f} embedded in a matrix with electric conductivity σ_{m} is considered here. This composite material may represent an idealized model of a biological tissue comprising tubular cells, such as skeletal muscle. Indeed, fibres and matrix model the intra- and extra-cellular phases, respectively, whose dielectric properties are negligible in the radio-frequency range [6]. Cells are coated by plasma membranes, which are dielectric lipid bilayers. Their thickness t is of the order of ten nanometres, much smaller than the spatial period L of the microstructure, which is of the order of tens of micrometres. Consequently, plasma membranes can be preferably modelled as two-dimensional interfaces between the intra- and extra-cellular phases, with conductance G and capacitance C per unit area, respectively given by the electric conductivity σ_{b} and permittivity ε_{b} of the bilayer, divided by its thickness [39]. Hence, the interface admittance per unit area is $Y = G + \mathrm{i}\omega C$ in the Fourier domain, where ω is the circular frequency. This finite interface admittance causes the electric potential to jump across the interfaces, so that they are usually referred to as imperfect.

In clinical applications, electric current is applied to body segments having sizes of centimetres to tens of centimetres, and its wavelength is of the same order in the radio-frequency range [2]. This suggests that the electric conduction problem can be studied by homogenization, in this frequency range [40]. To this end, a family of problems is introduced, indexed by a parameter ε scaling the microstructure (figure 1(*a*)). The value $\varepsilon = 1$ refers to the real composite material under consideration, whereas the homogenization limit is obtained by letting the parameter ε go to zero.

The problem of determining the electric potential u_ε in the composite with ε-scaled microstructure can be mathematically stated as follows [39, 41]:

$$-\mathrm{div}(\sigma \nabla u_\varepsilon) = 0, \qquad \text{in } \Omega_{\mathrm{f}}^{\varepsilon} \cup \Omega_{\mathrm{m}}^{\varepsilon}, \tag{1}$$

$$[\![\sigma \nabla u_\varepsilon \cdot \nu]\!] = 0, \qquad \text{on } \Gamma^{\varepsilon}, \tag{2}$$

$$\frac{Y}{\varepsilon}[\![u_\varepsilon]\!] = \sigma \nabla u_\varepsilon \cdot \nu, \qquad \text{on } \Gamma^{\varepsilon}, \tag{3}$$

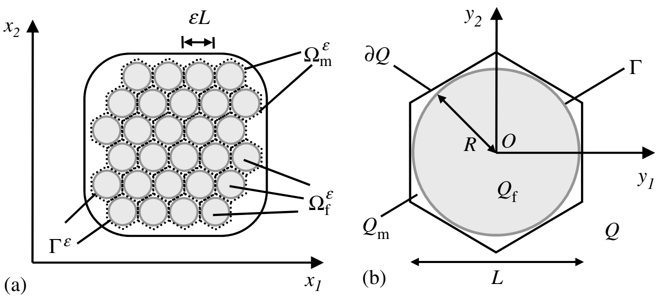

Figure 1. (*a*) Geometrical setting of the problem at the macroscale: cross section of the fibrous composite (the fibre size is exaggerated with respect to the sample size, for illustrative purposes).
(*b*) Geometrical setting of the cell (or local) problem at the microscale.

where Ω_f^ε and Ω_m^ε denote fibres and matrix, respectively; Γ^ε is the ensemble of interfaces (figure 1(*a*)); div and ∇ are the divergence and gradient operators, respectively; a dot denotes the scalar product; ν is the normal unit vector to Γ^ε pointing into Ω_m^ε; shadow brackets $[\![\cdot]\!]$ denote the jump of the enclosed quantity across the interface; finally, $\sigma = \sigma_f$ in Ω_f^ε, $\sigma = \sigma_m$ in Ω_m^ε. The quantities L, G, C, σ_f and σ_m are positive constants.

Equation (1) governs the Ohmic conduction in fibres and matrix; equation (2) accounts for the continuity of the current flux density across interfaces; equation (3) describes their electric capacitive/conductive behaviour. The quasi-static approximation of the Maxwell equations holds [2].

2.1. The homogenized equation

The asymptotic homogenization method [24, 25] is employed to find the overall complex conductivity of the tissue. It is only sketched here for the sake of completeness, since it is a standard technique. As shown in figure 1(*a*), two different scales characterize the problem. Hence, two different space variables are introduced: the macroscopic one, x, and the microscopic one, $y = x/\varepsilon$, $y \in Q$, Q being the unit cell. Accordingly, it turns out that [25]

$$\mathrm{div} = \frac{1}{\varepsilon}\mathrm{div}_y + \mathrm{div}_x, \qquad \nabla = \frac{1}{\varepsilon}\nabla_y + \nabla_x. \tag{4}$$

A formal asymptotic expansion is looked for in the form:

$$u_\varepsilon(x, y) = u_0(x, y) + \varepsilon u_1(x, y) + \varepsilon^2 u_2(x, y) + \cdots, \tag{5}$$

where u_0, u_1 and u_2 are Q-periodic in y, and u_1, u_2 have null integral average over Q. Substituting (5) into problem (1)–(3) and equating the power-like terms of ε, three differential problems for u_0, u_1 and u_2 are obtained. Considering the terms of order ε^{-2}, it turns out that

$$-\sigma\Delta_y u_0 = 0, \qquad \text{in } Q_f \cup Q_m, \tag{6}$$

$$[\![\sigma\nabla_y u_0 \cdot \nu]\!] = 0, \qquad \text{on } \Gamma, \tag{7}$$

$$Y[\![u_0]\!] = \sigma\nabla_y u_0 \cdot \nu, \qquad \text{on } \Gamma, \tag{8}$$

where Q_f and Q_m denote the regions of Q, respectively occupied by fibre and matrix, and Γ is their interface (figure 1(*b*)). Problem (6)–(8) implies that $u_0 = u_0(x)$ [41]. With this in mind, taking into consideration the terms of order ε^{-1}, it follows that

$$-\sigma\Delta_y u_1 = 0, \qquad \text{in } Q_f \cup Q_m, \tag{9}$$

$$[\![\sigma(\nabla_y u_1 + \nabla_x u_0) \cdot \nu]\!] = 0, \qquad \text{on } \Gamma, \tag{10}$$

$$Y[\![u_1]\!] = \sigma(\nabla_y u_1 + \nabla_x u_0) \cdot \nu, \qquad \text{on } \Gamma. \tag{11}$$

Finally, considering the terms of order ε^0, the problem for u_2 is obtained:

$$-\sigma\left(\Delta_y u_2 + 2\frac{\partial^2 u_1}{\partial x_j \partial y_j} + \Delta_x u_0\right) = 0, \quad \text{in } Q_f \cup Q_m, \tag{12}$$

$$[\![\sigma(\nabla_y u_2 + \nabla_x u_1) \cdot \nu]\!] = 0, \qquad \text{on } \Gamma, \tag{13}$$

$$Y[\![u_2]\!] = \sigma(\nabla_y u_2 + \nabla_x u_1) \cdot \nu, \qquad \text{on } \Gamma, \tag{14}$$

where the summation convention is adopted. Integrating (12) both in Q_f and in Q_m, using the Gauss–Green lemma, adding the two contributions and exploiting (13), the following equation is obtained:

$$\overline{\sigma}\Delta_x u_0 = \frac{1}{|Q|}\int_\Gamma [\![\sigma\nabla_x u_1 \cdot \nu]\!]\,\mathrm{d}\ell, \tag{15}$$

in which $\overline{\sigma} = (\sigma_f|Q_f| + \sigma_m|Q_m|)/|Q|$, $\mathrm{d}\ell$ is the line element of Γ and $|\cdot|$ denotes the Lebesgue measure. The unknown function u_1 is represented in the form [24, 25]:

$$u_1(x, y) = -\boldsymbol{\chi}(y) \cdot \nabla u_0(x), \tag{16}$$

where the complex-valued cell function $\boldsymbol{\chi}(y)$ has been introduced. Its components χ_h, $h = 1, 2$, are the unique null average Q-periodic solutions of the cell problem:

$$-\sigma\Delta_y \chi_h = 0, \qquad \text{in } Q_f \cup Q_m, \tag{17}$$

$$[\![\sigma(\nabla_y \chi_h - \boldsymbol{e}_h) \cdot \nu]\!] = 0, \qquad \text{on } \Gamma, \tag{18}$$

$$Y[\![\chi_h]\!] = \sigma(\nabla_y \chi_h - \boldsymbol{e}_h) \cdot \nu, \qquad \text{on } \Gamma, \tag{19}$$

where $\boldsymbol{e}_h$ is the unit vector parallel to the y_h axis, and can be regarded as a unit macroscopic electric field applied to the body. Hence, $-\nabla_y \chi_h$ is the corresponding perturbation field generated by interfacial polarization due to the microstructure.

Substituting (16) into (15), the homogenized equation for u_0 is finally derived:

$$-\,\mathrm{div}(\sigma^\#\nabla_x u_0) = 0. \tag{20}$$

Here $\sigma^\#$ is the homogenized admittance matrix, whose coefficients $(\sigma^\#)_{h,j}$, $h, j = 1, 2$, are given by

$$(\sigma^\#)_{h,j} = \overline{\sigma}\delta_{h,j} + \frac{1}{|Q|}\int_\Gamma [\![\sigma\chi_j]\!]\nu_h\,\mathrm{d}\ell, \tag{21}$$

where δ is the Krönecker symbol. Equation (21) yields the effective complex conductivity of the composite material in terms of the solution of the cell problem.

3. The cell problem

In this section a series solution to the cell problem (17)–(19) is obtained, and an analytical expression for the effective complex conductivity is derived.

3.1. Power series representation

The microstructure considered in this work (figure 1(*b*)) is invariant with respect to rotation of $\pi/3$ radians about the origin O. Hence, it can be proved that the unknowns χ_h, $h = 1, 2$, satisfy the following relation, for every $(y_1, y_2) \in Q$:

$$\frac{1}{2}\chi_1(y_1, y_2) + \frac{\sqrt{3}}{2}\chi_2(y_1, y_2) = \chi_1\left(\frac{1}{2}y_1 + \frac{\sqrt{3}}{2}y_2, -\frac{\sqrt{3}}{2}y_1 + \frac{1}{2}y_2\right). \quad (22)$$

As a consequence, only the cell function χ_1 needs to be determined. For the sake of simplicity, it is denoted by χ in the following. Moreover, the microstructure is invariant with respect to reflections about the y_1 and y_2 axes, so that χ turns out to be an odd (respectively, even) function with respect to y_1 (respectively, y_2). In particular, these properties, together with (22) and (21), imply that $\sigma^\#$ is a scalar matrix, and thus the homogenized material exhibits isotropic overall conductive behaviour in the plane orthogonal to the fibres.

Exploiting field equation (17) and the cited evenness and oddness properties, the unknown potential χ can be represented as follows:

- in the fibre (Q_f):

$$\chi(r,\theta)|_{Q_\mathrm{f}} := \chi_\mathrm{f}(r,\theta) = \sum_{k=1}^{+\infty}{}^{\mathrm{o}}\, a_k\left(\frac{r}{R}\right)^k \cos k\theta\,; \quad (23)$$

- in the matrix (Q_m):

$$\chi(r,\theta)|_{Q_\mathrm{m}} := \chi_\mathrm{m}(r,\theta) = \sum_{k=1}^{+\infty}{}^{\mathrm{o}}\left[b_k\left(\frac{r}{R}\right)^k + b_{-k}\left(\frac{r}{R}\right)^{-k}\right]\cos k\theta, \quad (24)$$

where (r,θ) are polar coordinates centred at the origin O, and the sums affected by the apex $^{\mathrm{o}}$ are carried out over odd indices only. As usual, only positive powers of r are taken in (23) due to regularity requirements, since Q_f contains the origin. The quantities a_k, b_k, b_{-k}, $k = 1, \ldots, +\infty$, odd k, are complex constants which will be determined by exploiting both the interface boundary conditions (18) and (19) on Γ, and the periodicity requirement on ∂Q.

3.2. Interface boundary conditions

Substituting (23) and (24) into (18) and (19) yields, for odd natural k:

$$\sigma_\mathrm{m}(kR^{-1}b_k - kR^{-1}b_{-k} - \delta_{k1}) = \sigma_\mathrm{f}(kR^{-1}a_k - \delta_{k1}), \quad (25)$$

$$Y(b_k + b_{-k} - a_k) = \sigma_\mathrm{f}(kR^{-1}a_k - \delta_{k1}). \quad (26)$$

These equations allow one to express a_k and b_k as linear functions of b_{-k}, $k = 1, \ldots, +\infty$, odd k, as follows:

$$a_k = \lambda_k b_{-k} + R\delta_{k1}, \quad (27)$$

$$b_k = \gamma_k b_{-k} + R\delta_{k1}, \quad (28)$$

where

$$\gamma_k = (\alpha + k)/(\beta + k), \qquad \lambda_k = 2RY\sigma_\mathrm{f}^{-1}/(\beta + k),$$
$$\alpha = RY(\sigma_\mathrm{f}^{-1} + \sigma_\mathrm{m}^{-1}), \qquad \beta = RY(\sigma_\mathrm{f}^{-1} - \sigma_\mathrm{m}^{-1}). \quad (29)$$

3.3. Periodic boundary conditions

The periodicity requirement on ∂Q is enforced by resorting to the theory of elliptic functions [26–28]. In particular, the function χ_m is represented as follows [29]:

$$\chi_\mathrm{m}(y_1, y_2) = -w_1\Re\left(\frac{\eta_1}{\omega_1}z\right) + \sum_{s=1}^{+\infty}{}^{\mathrm{o}}\, w_s\Re\left(\frac{\zeta^{(s-1)}(z)}{(s-1)!}\right), \quad (30)$$

where

$$z = (y_1 + \mathrm{i}y_2)/L \quad (31)$$

is the complex variable; $\mathrm{i} = \sqrt{-1}$ is the imaginary unit; $\Re(\cdot)$ denotes the real part; $\zeta(z)$, $\zeta^{(s)}(z)$ are the quasi-periodic Weierstrass Zeta function of semiperiods $\omega_1 = 1/2$ and $\omega_2 = \exp(\mathrm{i}\pi/3)/2$ and its sth derivative, respectively; $\eta_1 = \zeta(\omega_1) = \pi/\sqrt{3}$; and the quantities w_s, $s = 1, \ldots, +\infty$, odd s, are complex constants to be determined. Only odd indices are taken in (30), in order to fulfil the evenness and oddness properties of $\chi_\mathrm{m}(y_1, y_2)$ recalled above.

Equation (30) indeed implements the periodic boundary conditions on ∂Q, since, exploiting (A.2), (A.3) and remembering that the derivatives of ζ are elliptic functions, from (30) it follows that

$$\chi_\mathrm{m}(y_1 + L, y_2) = \chi_\mathrm{m}(y_1, y_2) = \chi_\mathrm{m}\left(y_1 + \frac{1}{2}L, y_2 + \frac{\sqrt{3}}{2}L\right), \quad (y_1, y_2) \in Q. \quad (32)$$

3.4. Solution of the cell problem

The two representations of the function χ_m given in (24) and (30) must coincide. This condition is enforced by recasting the latter representation as a Laurent series, using (A.8). Recalling that the constants $\mu_{k,s}$ entering (A.8) and defined in (A.9) are real quantities, after some algebra it turns out that

$$\chi_\mathrm{m}(y_1, y_2) = -\frac{\eta_1}{\omega_1}w_1\Re(z) + \sum_{k=1}^{+\infty}{}^{\mathrm{o}}\left[w_k\Re(z^{-k}) - \left(\sum_{s=1}^{+\infty}{}^{\mathrm{o}}\,\mu_{k,s}w_s\right)\Re(z^k)\right]. \quad (33)$$

Comparing (24) and (33), and recalling (31), the following equations are obtained, for every odd natural number k:

$$\rho^{-k}b_k = -\frac{\eta_1}{\omega_1}\delta_{k1}w_1 - \sum_{s=1}^{+\infty}{}^{\mathrm{o}}\,\mu_{k,s}w_s, \quad (34)$$

$$\rho^k b_{-k} = w_k, \quad (35)$$

where the dimensionless fibre radius was introduced:

$$\rho = \frac{R}{L}. \quad (36)$$

Substituting b_k and b_{-k} from (34) and (35) into (28), the following infinite system of linear equations for the unknowns w_k, $k = 1, \ldots, +\infty$, odd k, is obtained:

$$\rho^{-k}\gamma_k w_k + \rho^k\sum_{s=1}^{+\infty}{}^{\mathrm{o}}\,\mu_{k,s}w_s + \frac{\rho\eta_1}{\omega_1}\delta_{k1}w_1 = -R\delta_{k1}. \quad (37)$$

It is convenient [32] to rewrite the above system in terms of another set of variables y_k, $k = 1, \ldots, +\infty$, odd k:

$$y_k = \frac{\sqrt{k}}{\rho^k} w_k. \tag{38}$$

After some algebra, the following equation is derived:

$$\left(\boldsymbol{I} + \frac{\eta_1 \rho^2}{\gamma_1 \omega_1} \boldsymbol{u} \otimes \boldsymbol{u} + \boldsymbol{W\Gamma}^{-1} \right) \boldsymbol{\Gamma y} = -R\boldsymbol{u}, \tag{39}$$

where the unknowns y_k have been arranged into a vector $\boldsymbol{y}$, the vector $\boldsymbol{u}$ has the only nonzero element $u_1 = 1$, $\boldsymbol{I}$ is the identity matrix, $\otimes$ denotes the tensor product, $\boldsymbol{\Gamma}$ is a diagonal complex matrix having diagonal entries γ_k, $\boldsymbol{\Gamma}^{-1}$ is its inverse and the generic element $W_{k,s}$ of the real matrix $\boldsymbol{W}$ is $\mu_{k,s}\rho^{k+s}\sqrt{k/s}$, for odd natural numbers k, s. It can be shown that $\boldsymbol{W}$ is a symmetric matrix.

Equation (39) yields the unknowns y_k, for odd natural k, which in turn give the unknowns w_k, b_{-k}, b_k and a_k, respectively by (38), (35), (28) and (27). The latter quantities determine the cell function χ.

3.5. Effective complex conductivity

The effective complex conductivity is then computed by substituting the representations (23) and (24) of the cell function into (21). After some algebra, the following expression is obtained:

$$\sigma^\# = \overline{\sigma} + [\sigma_m(b_1 + b_{-1}) - \sigma_f a_1]\pi R/|Q| = \sigma_m[1 + 2py_1/R], \tag{40}$$

where

$$p = \frac{2\pi\rho^2}{\sqrt{3}} = \frac{\eta_1 \rho^2}{\omega_1} \tag{41}$$

is the fibre volume fraction. The matrix appearing in (21) has here been identified with the scalar $\sigma^\#$, since the homogenized material is isotropic in the plane orthogonal to the fibres.

It remains to estimate the quantity y_1 entering the above equation. To this end, it is necessary to truncate the infinite system (39) to a finite order N. Then, a numerical solution can be easily obtained, e.g. via a standard LU-decomposition.

Here a closed-form analytic solution is obtained. By applying Cramer's rule, from (39) it follows that

$$\frac{\sigma^\#}{\sigma_m} = 1 - \frac{2p}{\gamma_1}\left(\frac{-\gamma_1 y_1}{R}\right) = \frac{\det\left[\boldsymbol{I} - \dfrac{p}{\gamma_1}\boldsymbol{u}\otimes\boldsymbol{u} + \boldsymbol{W\Gamma}^{-1}\right]_N}{\det\left[\boldsymbol{I} + \dfrac{p}{\gamma_1}\boldsymbol{u}\otimes\boldsymbol{u} + \boldsymbol{W\Gamma}^{-1}\right]_N}, \tag{42}$$

where det denotes the determinant and suffix N denotes the truncation to the order N. Then, recalling the definitions of $\boldsymbol{W}$, $\boldsymbol{\Gamma}$, $\boldsymbol{u}$, and using a result from linear algebra reported in (B.2), the following closed-form formula is obtained:

$$\frac{\sigma^\#}{\sigma_m} = \frac{\gamma_1^- \sum_{n=0}^N \sum_{I\in{}_N\mathcal{C}_n} (\det \boldsymbol{M}_{I,I}) \left(\dfrac{\omega_1}{\eta_1}p\right)^{|I|} \prod_{k\in I} (\gamma_k^-)^{-1}}{\gamma_1^+ \sum_{n=0}^N \sum_{I\in{}_N\mathcal{C}_n} (\det \boldsymbol{M}_{I,I}) \left(\dfrac{\omega_1}{\eta_1}p\right)^{|I|} \prod_{k\in I} (\gamma_k^+)^{-1}}. \tag{43}$$

Here $\gamma_k^\pm = \gamma_k$, odd k, with the exception of $\gamma_1^\pm = \gamma_1 \pm p$, where the dimensionless parameters γ_k are defined in (29); ${}_N\mathcal{C}_n$ is the set of the combinations of the N odd indices $\{1, 3, \ldots, 2N-1\}$ taken n at a time; $\boldsymbol{M}$ is the matrix with elements $\mu_{k,s}$ defined in (A.9), for odd k, s; $\boldsymbol{M}_{I,I}$ is the principal minor of $\boldsymbol{M}$ corresponding to the rows and the columns with index in the subset I; finally, $|I|$ is the sum of the elements of I. The convention that $\det \boldsymbol{M}_{I,I} = 1$ and $\prod_{k\in I}(\gamma_k^\pm)^{-1} = 1$, if I is the empty set, is adopted. For the periodic hexagonal arrangement of circular cylinders considered herein, it results that $\omega_1/\eta_1 = \sqrt{3}/(2\pi)$.

Equation (43) has been derived under the hypothesis that σ_f and σ_m are real quantities, amounting to neglecting the permittivities of fibres and matrix. Nonetheless, (43) holds also when the latter hypothesis is not fulfilled, by replacing the real conductivities σ_f and σ_m with their complex counterparts [6] in the expression (29) of the constants γ_k.

Besides its theoretical interest, (43) supplies a hierarchy of simple explicit formulae, yielding better and better approximations of the effective complex conductivity, for larger and larger values of the truncation order N. As an example, taking $N = 1$ in (43) and recalling that $\mu_{1,1} = 0$, the following Maxwell–Garnett-type estimate for $\sigma^\#$ is obtained:

$$\frac{\sigma^\#}{\sigma_m} = \frac{\gamma_1^-}{\gamma_1^+} = 1 - \frac{2p}{\gamma_1}\left[1 + \frac{p}{\gamma_1}\right]^{-1}. \tag{44}$$

The same expression as above is obtained by taking $N = 2$. Then, taking $N = 3$ it turns out that

$$\frac{\sigma^\#}{\sigma_m} = 1 - \frac{2p}{\gamma_1}\left[1 + \frac{p}{\gamma_1} - \frac{f_{1,5}p^6}{\gamma_1\gamma_5}\right]^{-1}, \tag{45}$$

where $f_{1,5} = (\omega_1/\eta_1)^6 \mu_{1,5}\mu_{5,1} \approx 7.542\,217\,32 \times 10^{-2}$. Moreover, taking $N = 4$ it follows that

$$\frac{\sigma^\#}{\sigma_m} = 1 - \frac{2p}{\gamma_1}\left[1 + \frac{p}{\gamma_1} - \frac{\dfrac{f_{1,5}p^6}{\gamma_1\gamma_5}}{1 - \dfrac{f_{5,7}p^{12}}{\gamma_5\gamma_7}}\right]^{-1}, \tag{46}$$

where $f_{5,7} = (\omega_1/\eta_1)^{12}\mu_{5,7}\mu_{7,5} \approx 1.060\,283\,33$. The same expression as above is obtained by taking $N = 5$. Finally, taking $N = 6$ it follows that

$$\frac{\sigma^\#}{\sigma_m} = 1 - \frac{2p}{\gamma_1} \times \left[1 + \frac{p}{\gamma_1} - \frac{\dfrac{f_{1,5}p^6}{\gamma_1\gamma_5} + \dfrac{f_{1,11}p^{12}}{\gamma_1\gamma_{11}} - \dfrac{f_{1,5,7,11}p^{24}}{\gamma_1\gamma_5\gamma_7\gamma_{11}}}{1 - \dfrac{f_{5,7}p^{12}}{\gamma_5\gamma_7} - \dfrac{f_{7,11}p^{18}}{\gamma_7\gamma_{11}}}\right]^{-1}, \tag{47}$$

where $f_{1,11} = (\omega_1/\eta_1)^{12}\mu_{1,11}\mu_{11,1} \approx 7.649\,951\,87 \times 10^{-5}$, $f_{7,11} = (\omega_1/\eta_1)^{18}\mu_{7,11}\mu_{11,7} \approx 7.321\,003\,87 \times 10^{-1}$, and $f_{1,5,7,11} = (\omega_1/\eta_1)^{24}(\mu_{1,5}\mu_{5,1}\mu_{7,11}\mu_{11,7} + \mu_{1,11}\mu_{11,1}\mu_{5,7}\mu_{7,5} - \mu_{1,11}\mu_{11,7}\mu_{7,5}\mu_{5,1} - \mu_{1,5}\mu_{5,7}\mu_{7,11}\mu_{11,1}) \approx 5.106\,513\,36 \times 10^{-2}$.

Formulae analogous to (44)–(46) were derived in [31, 42], respectively in the cases of two-phase or three-phase composites with perfect interfaces, and an approximation of (47) up to the twelfth-order in p was derived in [43]. An equation analogous to (46) was obtained in [35] for square arrays of cylinders with interfacial contact resistance. To the authors' knowledge, the general formula (43) is presented here for the first time.

3.6. Distribution of relaxation times

The circular frequency ω enters (43) through the complex constants γ_k. A different expression for $\sigma^\#$ is derived here, aimed at emphasizing the dependence of $\sigma^\#$ on ω.

To this end, the Fourier coefficients $j_k := b_k + b_{-k} - a_k$ of the jump $[\![\chi]\!]$ of χ across Γ are introduced and arranged into a vector $\boldsymbol{j}$; analogously, the Fourier coefficients of the flux across Γ, reported on either side of (25), are arranged into a vector $\boldsymbol{f}$. Using (25), (34) and (35), the following equation is obtained:

$$\boldsymbol{f} = (\sigma_\mathrm{f}^{-1} + \sigma_\mathrm{m}^{-1})^{-1}(\boldsymbol{L}\,\boldsymbol{j}/R + 2\boldsymbol{v}), \tag{48}$$

where $\boldsymbol{L}$ is a positive self-adjoint operator and $\boldsymbol{v}$ is a vector, respectively defined by:

$$\boldsymbol{L} = \boldsymbol{N}^{\frac{1}{2}}(\boldsymbol{I} + \kappa\overline{\boldsymbol{W}})^{-1}(\boldsymbol{I} + \overline{\boldsymbol{W}})\boldsymbol{N}^{\frac{1}{2}},$$
$$\boldsymbol{v} = \boldsymbol{N}^{\frac{1}{2}}(\boldsymbol{I} + \kappa\overline{\boldsymbol{W}})^{-1}\boldsymbol{N}^{-\frac{1}{2}}\boldsymbol{u}. \tag{49}$$

Here $\kappa = (\sigma_\mathrm{m} - \sigma_\mathrm{f})/(\sigma_\mathrm{m} + \sigma_\mathrm{f})$, $\boldsymbol{N}$ is a diagonal matrix having as diagonal elements the odd integer numbers $k = 1, 3, \ldots, +\infty$, and $\overline{\boldsymbol{W}} = \boldsymbol{W} + (\eta_1\rho^2/\omega_1)\boldsymbol{u} \otimes \boldsymbol{u}$. It is pointed out that, under the assumption that σ_f and σ_m are real quantities, (48) does not involve ω. The latter enters (26), which, combined with (48), leads to

$$(\alpha\boldsymbol{I} + \boldsymbol{L})\,\boldsymbol{j} = -2R\boldsymbol{v}, \tag{50}$$

whence $\boldsymbol{j}$ can be obtained. Then, the effective complex conductivity results from (40), after computing $\boldsymbol{y}$ by

$$\boldsymbol{y} = \frac{1}{2}\boldsymbol{N}^{-\frac{1}{2}}[(\boldsymbol{N} - \kappa\boldsymbol{L})\,\boldsymbol{j} - 2\kappa R\boldsymbol{v}], \tag{51}$$

which follows from (38), (25), (34) and (35).

From a computational point of view, this approach is not as suitable as the one presented in section 3.5. However, it enables a suggestive spectral solution. Indeed, denoting by $\{\boldsymbol{g}^{(1)}, \boldsymbol{g}^{(2)}, \ldots, \boldsymbol{g}^{(n)}, \ldots\}$ an orthonormal basis of eigenvectors of $\boldsymbol{L}$, and by $\{\lambda_1, \lambda_2, \ldots, \lambda_n, \ldots\}$ the corresponding eigenvalues, from (50) it turns out that

$$\boldsymbol{j} \cdot \boldsymbol{g}^{(n)} = -2R\frac{\boldsymbol{g}^{(n)} \cdot \boldsymbol{v}}{\alpha + \lambda_n}. \tag{52}$$

This solution, after substituting into (51) and (40), yields

$$\sigma^\# = \sigma_\infty - \sum_{n=1}^{+\infty} \frac{\Delta\sigma_n}{1 + \mathrm{i}\omega\tau_n}, \tag{53}$$

where

$$\frac{\sigma_\infty}{\sigma_\mathrm{m}} = 1 - 2p\sum_{n=1}^{+\infty}(\boldsymbol{g}^{(n)} \cdot \boldsymbol{v})\kappa g_1^{(n)},$$
$$\frac{\Delta\sigma_n}{\sigma_\mathrm{m}} = \frac{2p(1 - \kappa\lambda_n)(\boldsymbol{g}^{(n)} \cdot \boldsymbol{v})g_1^{(n)}}{\lambda_n + RG(\sigma_\mathrm{f}^{-1} + \sigma_\mathrm{m}^{-1})},$$
$$\tau_n = \frac{RC(\sigma_\mathrm{f}^{-1} + \sigma_\mathrm{m}^{-1})}{\lambda_n + RG(\sigma_\mathrm{f}^{-1} + \sigma_\mathrm{m}^{-1})}. \tag{54}$$

Equation (53) shows that the present theory accounts for countably many relaxation processes, with relaxation times τ_n and conductivity increments $\Delta\sigma_n$, $n = 1, 2, \ldots, +\infty$. The high-frequency effective conductivity is σ_∞; the low-frequency one is

$$\sigma_\mathrm{s} = \sigma_\infty - \sum_{n=1}^{+\infty}\Delta\sigma_n, \tag{55}$$

and the relative importance of each relaxation process is given by $\Delta\sigma_n/(\sigma_\infty - \sigma_\mathrm{s})$. These countably many relaxation processes are due to electric interactions between fibres, rigorously taken into account here in the framework of a periodic hexagonal arrangement of circular cylinders with interfacial impedance.

4. Validation, results and discussion

In this section, the effectiveness of the present analytical method is proved by convergence analysis and comparison with finite-element solutions and existing models. The distribution of relaxation times is also discussed. Eventually, a parametric analysis is presented.

4.1. Physical and dimensionless parameters

Computations are performed with reference to a periodic hexagonal arrangement of cylinders with interfacial impedance, having the following geometrical and material properties:

- characteristic microstructural dimension $L = 50\,\mu$m;
- fibre and matrix conductivities: $\sigma_\mathrm{f} = 0.5\,\mathrm{S\,m^{-1}}$ and $\sigma_\mathrm{m} = 2\,\mathrm{S\,m^{-1}}$, respectively;
- interface capacitance $C = 10^{-2}\,\mathrm{F\,m^{-2}}$;
- interface conductance $G = 5\,\mathrm{S\,m^{-2}}$.

For sufficiently high volume fractions (i.e. $p = 0.9$) this composite can be regarded as a model of skeletal muscle [44]. Also lower values of p are considered in the following, for the sake of comparison.

It turns out that $Y \approx \mathrm{i}\omega C$, since $G \ll C\omega$ in the radio-frequency range [6]. The characteristic frequency ω_c is the frequency at which the imaginary part $\Im(\sigma^\#)$ of the effective complex conductivity $\sigma^\#$ attains its maximum value; the corresponding value of $\sigma^\#$ is denoted by $\sigma^\#_\mathrm{c}$. For convenience, the following dimensionless quantities are introduced:

- conductivity contrast (or ratio) $\xi = \sigma_\mathrm{f}/\sigma_\mathrm{m}$;
- dimensionless (circular) frequency $\Omega = \omega CL/\sigma_\mathrm{m}$ (the dimensionless counterpart of ω_c is denoted by Ω_c);
- dimensionless effective complex conductivity $\sigma^\#/\sigma_\mathrm{m}$.

Table 1. Present theoretical solution. Minimum order N required to give the effective complex conductivity at characteristic frequency ($\sigma_c^{\#}$), to the relative accuracy of 10^{-2} (on the left) or 10^{-4} (on the right). N is listed for various values of the volume fraction p and of the conductivity contrast ξ.

	Relative accuracy $= 10^{-2}$					Relative accuracy $= 10^{-4}$				
	ξ					ξ				
p	0	10^{-1}	0.25	10	$+\infty$	0	10^{-1}	0.25	10	$+\infty$
0.30	1	1	1	1	1	1	1	1	1	1
0.60	1	1	1	1	1	3	3	3	3	3
0.70	3	3	3	1	1	4	4	4	4	4
0.80	3	3	3	3	3	7	6	6	4	4
0.85	4	4	3	3	3	9	7	7	7	7
0.87	6	4	4	3	3	10	10	9	7	7
0.88	7	4	4	4	4	13	12	10	9	9
0.89	9	6	4	4	4	16	13	13	10	10
0.90	13	9	7	4	4	27	21	18	13	13

Table 2. Present theoretical solution. Dimensionless characteristic frequency (Ω_c) and corresponding dimensionless effective complex conductivity ($\sigma_c^{\#}/\sigma_m$) as functions of the solution order N. For $N = 1, 2, \ldots, 6$, equations (44)–(47), special cases of the general equation (43), were employed. Volume fractions $p = 0.30, 0.60, 0.90$. Conductivity contrast $\xi = 0.25$.

	$p = 0.30$			$p = 0.60$			$p = 0.90$		
N	Ω_c	$\frac{\Re(\sigma_c^{\#})}{\sigma_m}$	$\frac{\Im(\sigma_c^{\#})}{\sigma_m}$	Ω_c	$\frac{\Re(\sigma_c^{\#})}{\sigma_m}$	$\frac{\Im(\sigma_c^{\#})}{\sigma_m}$	Ω_c	$\frac{\Re(\sigma_c^{\#})}{\sigma_m}$	$\frac{\Im(\sigma_c^{\#})}{\sigma_m}$
1, 2 (44)	0.7662	0.6167	0.0782	0.5786	0.3603	0.1103	0.4954	0.1757	0.1230
3 (45)	0.7662	0.6167	0.0782	0.5784	0.3592	0.1108	0.4951	0.1613	0.1290
4, 5 (46)	0.7662	0.6167	0.0782	0.5784	0.3592	0.1108	0.4956	0.1563	0.1328
6 (47)	0.7662	0.6167	0.0782	0.5784	0.3592	0.1108	0.4955	0.1553	0.1338
10	0.7662	0.6167	0.0782	0.5784	0.3592	0.1108	0.4949	0.1539	0.1354
15	0.7662	0.6167	0.0782	0.5784	0.3592	0.1108	0.4947	0.1538	0.1356
20	0.7662	0.6167	0.0782	0.5784	0.3592	0.1108	0.4946	0.1537	0.1356
25	0.7662	0.6167	0.0782	0.5784	0.3592	0.1108	0.4946	0.1537	0.1357

4.2. Convergence

As noted in section 3.5, it is necessary to truncate the infinite system (39) to a finite order N, amounting to taking into account a finite number N of coefficients in the representations (23) and (24) of the unknown electric potential.

Table 1 shows the minimum value of N required if the effective complex conductivity at characteristic frequency ($\sigma_c^{\#}$) is to have a relative accuracy of 10^{-2} (on the left) or 10^{-4} (on the right). This value increases with volume fraction p and decreases with conductivity contrast ξ. In particular, the well-known difficulty of convergence encountered at high volume fractions of highly conductive cylinders relative to the surrounding medium [37] is mitigated by the presence of imperfect interfaces.

Table 2 shows the dimensionless characteristic frequency Ω_c and the corresponding dimensionless effective complex conductivity $\sigma_c^{\#}/\sigma_m$, as functions of the order N of the solution. The reported values were obtained for contrast $\xi = 0.25$ and volume fractions $p = 0.30, 0.60, 0.90$. The convergence was very fast and just a few coefficients turned out to be sufficient in order to achieve good approximations. In particular, a relative error smaller than 2.1% (respectively, 1.4%) was obtained, even for $p = 0.90$, when the simple, closed-form expression (46) (respectively, (47)) was employed.

4.3. Comparison with FEM

Finite-element solutions of the cell problem (17)–(19) are presented here, for the sake of comparison. They were obtained by using the commercial code COMSOL 3.4 [45], which allows one to prescribe periodic boundary conditions on ∂Q, and to specify the model equations (17)–(19) using a weak formulation [46], especially suitable in order to account for the imperfect-interface condition (19).

Different meshes were considered. As an example, the one depicted in figure 2 is characterized by the mesh parameter $h/L = 0.05$, where h is the maximum element size. A number of layers of elements from 1 ($h/L = 0.1$) to 8 ($h/L = 0.0125$) were created in the narrow regions between the fibre Q_f and the periodic outer boundary ∂Q, by suitably setting the COMSOL mesh-generation parameters [45]. Coarser (respectively, finer) meshes were obtained by taking $h/L = 0.1$ (respectively, $h/L = 0.025, 0.0125$). Quadratic Lagrange triangular finite elements [46] were employed.

Table 3 shows the convergence of the finite-element solutions. The dimensionless characteristic frequency Ω_c and the corresponding dimensionless effective complex conductivity $\sigma_c^{\#}/\sigma_m$ are reported, as functions of the mesh parameter h/L. The simulations were carried out for contrast $\xi = 0.25$ and volume fractions $p = 0.30, 0.60, 0.90$. The adopted quadratic elements showed very good convergence properties. After the convergence is reached, a complete agreement with the analytical method presented herein (last line of table 2) is obtained. The latter, however, is computationally much less demanding.

4.4. Comparison with existing models

In this section the present theory is compared with existing models of the effective complex conductivity of cell suspensions. Herein the well-known PS [21] or HAK [22] models are considered. As a matter of fact, they are suitably modified in order to cover the present case of coated cylindrical inclusions.

In the spirit of [21,22], the effective complex conductivity of a coated cylinder is given by

$$\sigma_{\mathrm{cc}}^* = \sigma_{\mathrm{b}}^* \frac{(1-v)\sigma_{\mathrm{b}}^* + (1+v)\sigma_{\mathrm{f}}}{(1+v)\sigma_{\mathrm{b}}^* + (1-v)\sigma_{\mathrm{f}}}, \tag{56}$$

where $\sigma_{\mathrm{b}}^* = \mathrm{i}\omega\varepsilon_{\mathrm{b}}$ is the complex conductivity of the lipid bilayer, mainly exhibiting dielectric behaviour, $v = (1-t/R)^2$, and t is the coating thickness. Since t is three orders of magnitude smaller than the cylinder radius R, a simpler expression can be derived from (56) by introducing the interface admittance per unit area defined in section 2, $Y = \mathrm{i}\omega\varepsilon_{\mathrm{b}}/t$, and neglecting higher-order terms in t. Hence, the following expression is obtained [47]:

$$\sigma_{\mathrm{cc}}^* = \frac{\sigma_{\mathrm{f}}}{1+\sigma_{\mathrm{f}}/(RY)}. \tag{57}$$

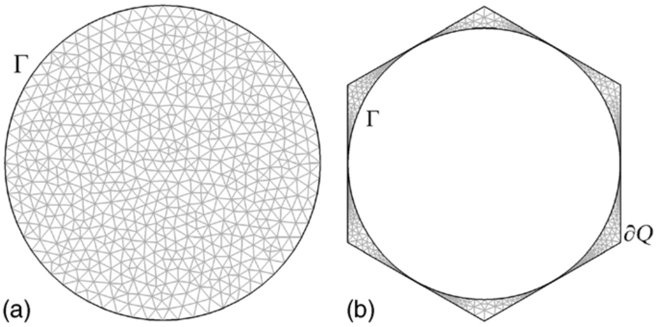

Figure 2. Example of finite-element mesh used in the computations: volume fraction $p = 0.90$; mesh parameter $h/L = 0.05$; element growth rate: 1.2; resolution of narrow regions: 2 [45]. (*a*) Fibre Q_{f}, with boundary Γ. (*b*) Matrix Q_{m}, with inner boundary Γ and periodic outer boundary ∂Q.

Equation (57) is then substituted into the Maxwell–Garnett equation, leading to a PS-type model [47]:

$$\sigma^{\#} = \sigma_{\mathrm{m}} \frac{(1-p)\sigma_{\mathrm{m}} + (1+p)\sigma_{\mathrm{cc}}^*}{(1+p)\sigma_{\mathrm{m}} + (1-p)\sigma_{\mathrm{cc}}^*}, \tag{58}$$

or into an analogue of Hanai's equation, suitably modified in order to take into account the cylindrical shape of cells, leading to a HAK-type model:

$$\frac{\sigma^{\#} - \sigma_{\mathrm{cc}}^*}{\sigma_{\mathrm{m}} - \sigma_{\mathrm{cc}}^*}\left(\frac{\sigma_{\mathrm{m}}}{\sigma^{\#}}\right)^{1/2} = 1 - p. \tag{59}$$

It turns out that (58) coincides with (44): indeed, the PS-type model is known to yield a first-order approximation of the effective complex conductivity.

Table 4 shows the dimensionless characteristic frequency Ω_{c} and the corresponding dimensionless effective complex conductivity $\sigma_{\mathrm{c}}^{\#}/\sigma_{\mathrm{m}}$, as computed according to the three models under comparison. The reported values were obtained for contrasts $\xi = 0, 0.25, +\infty$, and volume fractions $p = 0.30$, 0.60, 0.90. In the case $\xi = 0$ (i.e. nonconductive inclusions), the interface properties have no influence on the effective conductivity of the composite, which behaves like a purely conductive perforated domain.

The present results are close to the PS-type results at low volume fractions, where the latter are deemed to be satisfactory, and to the HAK-type results at high volume fractions, where the HAK theory is believed to behave better than the PS theory. The latter issue is further stressed in figure 3, relevant to volume fraction $p = 0.9$ and contrast $\xi = 0.25$. In particular, figures 3(*a*) and (*b*), respectively plot the real and imaginary parts of the dimensionless effective complex conductivity as functions of the dimensionless frequency Ω; figure 3(*c*) plots the dimensionless effective real permittivity $\Im(\sigma^{\#})/(\sigma_{\mathrm{m}}\Omega)$, also given by $\Im(\sigma^{\#})/(\omega CL)$, as a function of Ω. Finally, the conductivity locus is depicted in figure 3(*d*), where a remarkable agreement between the present theory and HAK model appears. An asset of the former is its ability to supply approximations of the effective conductivity in the form of rational expressions.

Figures 3(*a*)–(*c*) are also aimed at ascertaining the validity of neglecting the permittivities of fibres and matrix, by comparing the corresponding results (solid lines) to the ones obtained by replacing the real conductivities σ_{f} and σ_{m}, respectively with the complex conductivities $\sigma_{\mathrm{f}} + \mathrm{i}\omega\varepsilon_{\mathrm{r}}\varepsilon_0$ and $\sigma_{\mathrm{m}} + \mathrm{i}\omega\varepsilon_{\mathrm{r}}\varepsilon_0$ (dotted lines), where $\varepsilon_{\mathrm{r}} \approx 80$ [6] and ε_0 is

Table 3. Finite-element solutions. Dimensionless characteristic frequency (Ω_{c}) and corresponding dimensionless effective complex conductivity ($\sigma_{\mathrm{c}}^{\#}/\sigma_{\mathrm{m}}$), as functions of the mesh parameter h/L. Quadratic Lagrange triangular finite elements. Volume fractions $p = 0.30$, 0.60, 0.90. Conductivity contrast $\xi = 0.25$.

	$p = 0.30$			$p = 0.60$			$p = 0.90$		
$\frac{h}{L}$	Ω_{c}	$\frac{\Re(\sigma_{\mathrm{c}}^{\#})}{\sigma_{\mathrm{m}}}$	$\frac{\Im(\sigma_{\mathrm{c}}^{\#})}{\sigma_{\mathrm{m}}}$	Ω_{c}	$\frac{\Re(\sigma_{\mathrm{c}}^{\#})}{\sigma_{\mathrm{m}}}$	$\frac{\Im(\sigma_{\mathrm{c}}^{\#})}{\sigma_{\mathrm{m}}}$	Ω_{c}	$\frac{\Re(\sigma_{\mathrm{c}}^{\#})}{\sigma_{\mathrm{m}}}$	$\frac{\Im(\sigma_{\mathrm{c}}^{\#})}{\sigma_{\mathrm{m}}}$
0.1	0.7613	0.6152	0.0789	0.5784	0.3592	0.1108	0.4948	0.1538	0.1354
0.05	0.7626	0.6156	0.0787	0.5784	0.3592	0.1108	0.4947	0.1537	0.1356
0.025	0.7662	0.6167	0.0782	0.5784	0.3592	0.1108	0.4946	0.1537	0.1357
0.0125	0.7662	0.6167	0.0782	0.5784	0.3592	0.1108	0.4946	0.1537	0.1357

Table 4. Comparison among PS-type, HAK-type and present models. Dimensionless characteristic frequency (Ω_c) and corresponding dimensionless effective complex conductivity ($\sigma_c^\#/\sigma_m$). Volume fractions $p = 0.30,\ 0.60,\ 0.90$. Conductivity contrasts $\xi = 0, 0.25, +\infty$.

	$p = 0.30$			$p = 0.60$			$p = 0.90$		
Model	Ω_c	$\frac{\Re(\sigma_c^\#)}{\sigma_m}$	$\frac{\Im(\sigma_c^\#)}{\sigma_m}$	Ω_c	$\frac{\Re(\sigma_c^\#)}{\sigma_m}$	$\frac{\Im(\sigma_c^\#)}{\sigma_m}$	Ω_c	$\frac{\Re(\sigma_c^\#)}{\sigma_m}$	$\frac{\Im(\sigma_c^\#)}{\sigma_m}$
					$\xi = 0$				
PS-type	–	0.5385	0.	–	0.2500	0.	–	0.0526	0.
HAK-type	–	0.4900	0.	–	0.1600	0.	–	0.0100	0.
Present	–	0.5384	0.	–	0.2483	0.	–	0.0178	0.
					$\xi = 0.25$				
PS-type	0.7662	0.6167	0.0782	0.5786	0.3603	0.1103	0.4954	0.1757	0.1230
HAK-type	0.6821	0.5876	0.0953	0.4972	0.3102	0.1380	0.4692	0.1561	0.1333
Present	0.7662	0.6167	0.0782	0.5784	0.3592	0.1108	0.4946	0.1537	0.1357
					$\xi = +\infty$				
PS-type	6.4579	1.1978	0.6593	9.8356	2.1250	1.8750	38.145	9.5263	9.4737
HAK-type	9.1504	1.3273	0.6410	26.354	3.5033	2.5006	388.71	53.597	42.623
Present	6.4574	1.1978	0.6593	9.9333	2.1327	1.8660	305.17	32.192	21.945

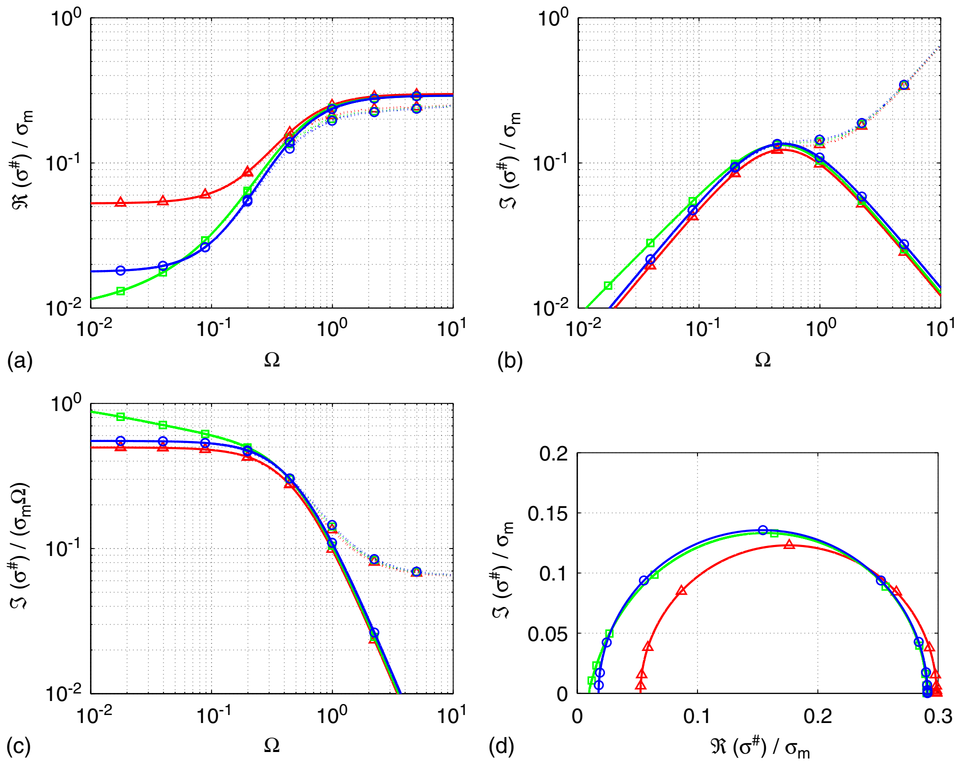

Figure 3. (*a*) Real part and (*b*) imaginary part of dimensionless effective complex conductivity versus dimensionless frequency. (*c*) Dimensionless effective permittivity versus dimensionless frequency. (*d*) Imaginary versus real part of dimensionless effective complex conductivity. The permittivities of fibres and matrix are neglected (solid lines) or taken into account (dotted lines). Volume fraction $p = 0.9$; contrast $\xi = 0.25$. Present model: blue/circles; PS-type model: red/triangles up; HAK-type model: green/squares.

the permittivity of vacuum. It turns out that neglecting the permittivities yields satisfactory results up to a dimensionless frequency of the order of unity, corresponding to about 1 MHz in physical units. Above that value, complex conductivities should be considered; however, the present treatment would remain unchanged.

4.5. Distribution of relaxation times

It is shown in section 3.6 that the present theory accounts for countably many relaxation processes, arising even when σ_f and σ_m are real quantities. Their significance is investigated in this section. Table 5 gives the high- and low-frequency dimensionless conductivities σ_∞/σ_m and σ_s/σ_m, respectively, the relative magnitudes $\Delta\sigma_n/(\sigma_\infty - \sigma_s)$ of the first three most relevant relaxation processes, and the corresponding dimensionless relaxation times $\tau_n\sigma_m/(CL)$, for volume fractions $p = 0.30,\ 0.60,\ 0.90$ and conductivity contrast $\xi = 0.25$. It can be observed that one relaxation process is prevailing, accounting alone for over 97% of the total conductivity increment from low to high frequencies, even for $p = 0.9$.

Table 5. Present theoretical solution. High- and low-frequency dimensionless conductivities σ_∞/σ_m and σ_s/σ_m, respectively. Dimensionless relaxation times $\tau_n\sigma_m/(CL)$ and corresponding relative conductivity increments $\Delta\sigma_n/(\sigma_\infty - \sigma_s)$ for $n = 1, 2, 3$. Finally, fitted Cole–Cole parameters: α and $\tau\sigma_m/(CL)$. Volume fractions $p = 0.30, 0.60, 0.90$. Conductivity contrast $\xi = 0.25$.

p	$\frac{\sigma_\infty}{\sigma_m}$	$\frac{\sigma_s}{\sigma_m}$	$\frac{\Delta\sigma_1}{\sigma_\infty-\sigma_s}$	$\frac{\tau_1\sigma_m}{CL}$	$\frac{\Delta\sigma_2}{\sigma_\infty-\sigma_s}$	$\frac{\tau_2\sigma_m}{CL}$	$\frac{\Delta\sigma_3}{\sigma_\infty-\sigma_s}$	$\frac{\tau_3\sigma_m}{CL}$	α	$\frac{\tau\sigma_m}{CL}$
0.30	0.6949	0.5384	1.0000	1.3052	1.6×10^{-5}	0.2876	1.4×10^{-11}	0.1307	7.2×10^{-5}	1.3051
0.60	0.4701	0.2483	0.9989	1.7297	0.0011	0.4077	4.5×10^{-7}	0.2904	4.2×10^{-4}	1.7279
0.90	0.2911	0.0178	0.9764	2.0458	0.0221	0.8357	0.0015	0.3933	0.0048	2.0097

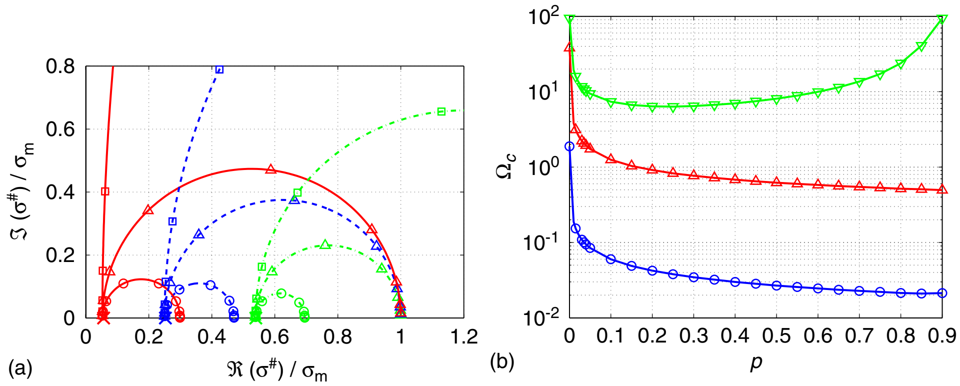

Figure 4. (*a*) Imaginary versus real part of dimensionless effective complex conductivity for different volume fractions and contrasts. Volume fraction $p = 0.30$: green - · -; $p = 0.60$: blue - - -; $p = 0.90$: red —. Contrast $\xi = 0$: crosses; $\xi = 0.25$: circles; $\xi = 1$: triangles up; $\xi = +\infty$: squares. (*b*) Dimensionless characteristic frequency versus volume fraction for different contrasts. Contrast $\xi = 0.25$: blue/circles; $\xi = 1$: red/triangles up; $\xi = +\infty$: green/triangles down.

This issue is further stressed by fitting Cole–Cole depressed circles [8], given by

$$\sigma^\# = \sigma_\infty + \frac{\sigma_s - \sigma_\infty}{1 + (i\omega\tau)^{1-\alpha}}, \tag{60}$$

to the theoretically computed conductivity loci. The fitted values of the distribution parameter α, which is a measure of the broadening of the dispersion, and of the dimensionless characteristic relaxation time τ, are reported in the last two columns of table 5.

The prevalence of one relaxation process, or else the small value of α obtained by fit, implies that electric interactions between fibres can only partially account, in the framework of a periodic hexagonal arrangement of circular cylinders with interfacial impedance, for the experimentally observed broadening of the distribution of relaxation times in real tissues [9]. A rigorous micromechanical model able to capture the latter issue may require taking into account geometrical features of real tissues, such as irregular cell shape or distribution of cell size. This is beyond the scope of this work, but the present approach could be extended to deal with those situations.

4.6. Parametric analysis

A parametric analysis may be useful to assess the effect of microstructural parameters on the effective complex conductivity of the composite.

Figure 4(*a*) shows the dimensionless effective conductivity loci obtained for different values of volume fraction ($p = 0.30, 0.60, 0.90$) and contrast ($\xi = 0, 0.25, 1, +\infty$). As discussed above, for $\xi \neq 0$ the locus is approximately an arc of circle in which frequency increases from left to right. The imaginary part of $\sigma^\#/\sigma_m$, as resulting from interfacial polarization, vanishes at very low or very high frequencies, since in those situations capacitive interfaces act as open or short circuits, respectively. Moreover at very low frequencies, for fixed volume fraction p, curves relevant to different contrasts ξ originate from the same point on the real axis, corresponding to the effective real conductivity of a perforated domain. In particular, for $\xi = 0$ (i.e. nonconductive inclusions) the locus collapses to that point, which moves left as the volume fraction increases. For $\xi = 1$ (i.e. the same conductivity of fibres and matrix) the effect of the volume fraction disappears at very high frequencies, where interfaces become perfect and the composite behaves like a homogeneous material with $\sigma^\#/\sigma_m = 1$.

The behaviour of the dimensionless characteristic frequency Ω_c as a function of the volume fraction is reported in figure 4(*b*), for contrasts $\xi = 0.25, 1, +\infty$. In particular, for $\xi = 0.25$ or $\xi = 1$, Ω_c is a decreasing function of p, whereas for $\xi = +\infty$ it attains a minimum at intermediate volume fractions.

In figure 5(*a*), the dimensionless effective complex conductivity is reported as a function of the volume fraction, at very low, very high or characteristic frequency, for contrast $\xi = 0.25$: as expected, it is purely real at extreme frequencies.

The curves in figures 4 and 5(*a*) show a sharp dependence of the effective complex conductivity and the characteristic frequency on the volume fraction and, hence, they may be useful in estimating the latter quantity, an issue which has clinical significance in situations implying changes in the body water content (e.g. during dialysis [48]).

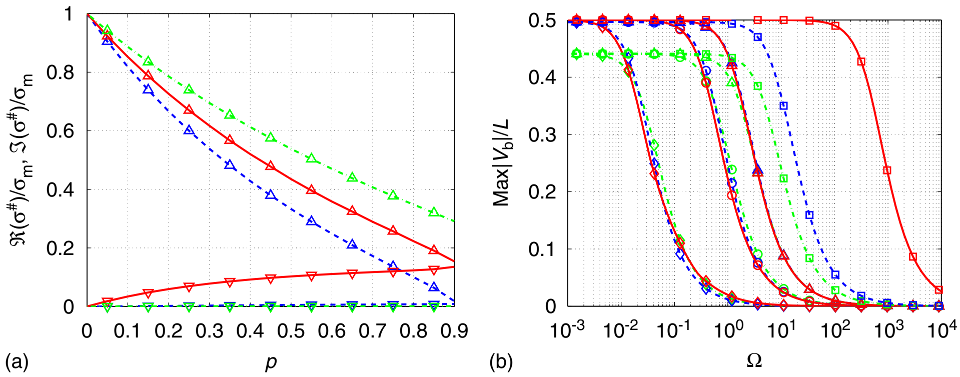

Figure 5. (*a*) Dimensionless effective complex conductivity versus volume fraction for contrast $\xi = 0.25$ and different dimensionless frequencies. Very low dimensionless frequency: green - · -; characteristic dimensionless frequency: red —; very high dimensionless frequency: blue - - -. Real (respectively, imaginary) part: triangles up (respectively, down). (*b*) Maximum dimensionless membrane potential versus dimensionless frequency for different volume fractions and contrasts. Volume fraction $p = 0.30$: green - · -; $p = 0.60$: blue - - -; $p = 0.90$: red —. Contrast $\xi = 0$: diamonds; $\xi = 0.25$: circles; $\xi = 1$: triangles up; $\xi = +\infty$: squares.

During impedance spectroscopy measurements, an estimate of the electric potential induced across the lipid bilayer by the radio-frequency current injection may be useful to assess the risk of muscle excitement. The induced potential per unit macroscopic electric field is given by $V_b = [\![\chi]\!]$; its dimensionless counterpart is V_b/L. The maximum value of $|V_b|/L$ as a function of the dimensionless frequency is depicted in figure 5(*b*), for volume fractions $p = 0.30$, 0.60, 0.90, and contrasts $\xi = 0$, 0.25, 1, $+\infty$. In all cases the trend is sigmoidal: the induced potential vanishes at high frequencies, due to interfaces acting as a short circuit, and reaches a plateau at low frequencies. In physical units, the latter, slightly depending on the volume fraction, is of the order of one-half the microstructural characteristic length times the macroscopic electric field.

5. Conclusions

In this work, dielectric properties of a periodic fibrous composite with interfacial impedance and hexagonal symmetry were investigated. The asymptotic homogenization method was used and an analytical solution to the local problem was found by employing Weierstrass elliptic functions. This approach led to a simple closed-form formula for the effective complex conductivity of the composite. Finite-element solutions were used as a benchmark for validation. A parametric analysis pointed out the dependence of the effective complex conductivity on the microstructure.

The composite material studied herein is an idealization of a biological tissue comprising tubular cells, such as skeletal muscle. The present results may help in understanding dielectric properties of the latter, notwithstanding its extreme structural complexity. As an example, the present model was able to take rigorously into account electric interactions between fibres in the framework of a periodic hexagonal arrangement, and to ascertain their influence on the effective complex conductivity of the composite in the radio-frequency range.

Future research will consider different arrangements, uneven distribution of fibre size, irregular fibre shape and 3D geometries.

Acknowledgments

The authors express their sincere gratitude to Professor Franco Maceri for useful discussions and valuable advises. They thank the anonymous referees for constructive criticism.

Appendix A. Some results from the elliptic function theory

The Weierstrass Zeta function of semiperiods ω_1, ω_2, is defined by [26–28]

$$\zeta(z) = \frac{1}{z} + {\sum_{m,n}}' \left(\frac{1}{z - \Omega_{m,n}} + \frac{1}{\Omega_{m,n}} + \frac{z}{\Omega_{m,n}^2} \right), \qquad \text{(A.1)}$$

where $\Omega_{m,n} = 2m\omega_1 + 2n\omega_2$, for $m, n \in \mathbf{Z}$, and the apex over the summation symbol means that the pair $(m, n) = (0, 0)$ is excluded. The function $\zeta(z)$ is analytic over the whole z-plane, except at simple poles at all the points of the set $\Omega_{m,n}$; it is odd and quasi-periodic, that is

$$\zeta(z + 2\omega_k) = \zeta(z) + 2\eta_k, \qquad \text{(A.2)}$$

with $k = 1, 2$ and $\eta_k = \zeta(\omega_k)$. Its derivatives are elliptic functions. The following relationship links η_1, η_2 and the semiperiods ω_1, ω_2:

$$\eta_1\omega_2 - \eta_2\omega_1 = \frac{1}{2}\pi \mathrm{i}. \qquad \text{(A.3)}$$

The Laurent series expansion of ζ is

$$\zeta(z) = \frac{1}{z} - \sum_{k=2}^{+\infty} c_k \frac{z^{2k-1}}{2k-1}, \qquad \text{(A.4)}$$

where $c_2 = g_2/20$, $c_3 = g_3/28$, and

$$c_k = \frac{3}{(2k+1)(k-3)} \sum_{m=2}^{k-2} c_m c_{k-m}, \qquad k \geqslant 4. \qquad \text{(A.5)}$$

For ease of notation, it is stipulated that $c_1 = 0$. The quantities g_2 and g_3, known as invariants, are given by the equations

$$g_2 = 60{\sum_{m,n}}'(\Omega_{m,n})^{-4}, \qquad g_3 = 140{\sum_{m,n}}'(\Omega_{m,n})^{-6}. \tag{A.6}$$

An alternative expression for c_k, $k \geqslant 2$ is given by

$$\frac{c_k}{2k-1} = {\sum_{m,n}}'(\Omega_{m,n})^{-2k}$$
$$= 2(2\omega_1)^{-2k}\left[\zeta_R(2k) + \frac{(2\pi \mathrm{i})^{2k}}{(2k-1)!}\sum_{n=1}^{+\infty}\sigma_{2k-1}(n)\mathrm{e}^{2\pi \mathrm{i}n\omega_2/\omega_1}\right], \tag{A.7}$$

where $\zeta_R(\alpha) = \sum_{n=1}^{+\infty} n^{-\alpha}$ is the Riemann Zeta function, and $\sigma_\alpha(n) = \sum_{l|n} l^\alpha$ is the divisor function.

The Laurent series expansion of the $(s-1)$th derivative of ζ, $s \geqslant 1$, odd s, is given by

$$\frac{\zeta^{s-1}(z)}{(s-1)!} = z^{-s} - \sum_{k=1}^{+\infty}\mu_{k,s}z^k, \tag{A.8}$$

where for odd natural numbers k, s,

$$\mu_{k,s} = \frac{1}{k+s-1}\binom{k+s-1}{s-1}c_{\frac{k+s}{2}}, \tag{A.9}$$

and round brackets denote the binomial coefficient. In particular, it turns out that $\mu_{1,1} = 0$. Moreover, if $\omega_2/\omega_1 = \exp(\mathrm{i}\pi/3)$, then $\mu_{k,s}$ vanishes when 6 does not divide $k+s$.

Appendix B. A result from linear algebra

For any square matrix $\boldsymbol{A}$ of order N, it is well known that

$$\det(\boldsymbol{I}+\boldsymbol{A}) = \sum_{n=0}^{N}\iota_n(\boldsymbol{A}) = \sum_{n=0}^{N}\sum_{I\in{}_N\mathcal{C}_n}\det\boldsymbol{A}_{I,I}, \tag{B.1}$$

where $\boldsymbol{I}$ is the identity matrix, det denotes the determinant, $\iota_n(\boldsymbol{A})$ is the nth invariant of $\boldsymbol{A}$, ${}_N\mathcal{C}_n$ is the set of the combinations of the indices $\{1, 2, \ldots, N\}$ taken n at a time and $\boldsymbol{A}_{I,I}$ is the principal minor of the matrix $\boldsymbol{A}$ corresponding to the rows and the columns with index in the subset I. It is understood that $\iota_0(\boldsymbol{A}) = 1$, and $\det\boldsymbol{A}_{I,I} = 1$ if I is the empty set. Consequently, it turns out that

$$\det(\boldsymbol{I}+\lambda\boldsymbol{u}\otimes\boldsymbol{u}+\boldsymbol{A}) = \sum_{n=0}^{N}\sum_{I\in{}_N\mathcal{C}_n}h(I)\det\boldsymbol{A}_{I,I}, \tag{B.2}$$

where λ is a scalar, $\boldsymbol{u}$ is the unit vector with the only nonzero element $u_1 = 1$ and

$$h(I) = \begin{cases} 1, & \text{if } 1 \in I, \\ 1+\lambda, & \text{if } 1 \notin I. \end{cases} \tag{B.3}$$

References

[1] Bayford R H 2006 Bioimpedance tomography (electrical impedance tomography) *Ann. Rev. Biomed. Eng.* **8** 63–91

[2] Cheney M, Isaacson D and Newell J C 1999 Electrical impedance tomography *SIAM Rev.* **41** 85–101

[3] Ellis K J 2000 Human body composition: *in vivo* methods *Physiol. Rev.* **80** 649–80

[4] Nenchev N, Hatib F and Daskalov I 1998 Monitoring relative fluid balance alterations in haemodialysis of diabetic patients by electrical impedance *Physiol. Meas.* **19** 35–52

[5] Ni Y, Mulier S, Miao Y, Michel L and Marchal G 2005 A review of the general aspects of radiofrequency ablation *Abdom. Imaging* **30** 381–400

[6] Foster K R and Schwan H P 1989 Dielectric properties of tissues and biological materials: a critical review *CRC Crit. Rev. Biomed. Eng.* **17** 25–104

[7] Debye P 1928 *Polar Molecules* (New York: Dover)

[8] Cole K S and Cole R H 1941 Dispersion and absorption in dielectrics: I. Alternating current characteristics *J. Chem. Phys.* **9** 341–51

[9] Gabriel S, Lau R W and Gabriel C 1996 The dielectric properties of biological tissues: III. Parametric models for the dielectric spectrum of tissues *Phys. Med. Biol.* **41** 2271–93

[10] Paulson K S, Jouravleva S and McLeod C N 2000 Dielectric relaxation time spectroscopy *IEEE Trans. Biomed. Eng.* **47** 1510–7

[11] Gimsa J and Wachner D 1998 A unified resistor–capacitor model for impedance, dielectrophoresis, electrorotation, and induced transmembrane potential *Biophys. J.* **75** 1107–16

[12] Gersing E 1998 Impedance spectroscopy of living tissue for determination of the state of organs *Bioelectrochem. Bioenerg.* **45** 145–9

[13] Zhu F, Leonard E F and Levin N W 2005 Body composition modeling in the calf using an equivalent circuit model of multy-frequency bioimpedance analysis *Physiol. Meas.* **26** S133–43

[14] McAdams E T and Jossinet J 1996 Problems in equivalent circuit modelling of the electrical properties of biological tissues *Bioelectrochem. Bioenerg.* **40** 147–52

[15] Asami K 2007 Dielectric properties of biological tissues in which cells are connected by communicating junctions *J. Phys. D: Appl. Phys.* **40** 3718–27

[16] Fear E C and Stuchly M A 1998 Modeling assemblies of biological cells exposed to electric fields *IEEE Trans. Biomed. Eng.* **45** 1259–71

[17] Foster K and Sowers A E 1995 Dielectrophoretic forces and potentials induced on pairs of cells in an electric field *Biophys. J.* **69** 777–84

[18] Asami K 2006 Dielectric dispersion in biological cells of complex geometry simulated by the three-dimensional finite difference method *J. Phys. D: Appl. Phys.* **39** 492–9

[19] Asami K 2006 Effects of membrane disruption on dielectric properties of biological cells *J. Phys. D: Appl. Phys.* **39** 4656–63

[20] Stewart D A Jr, Gowrishankar T R, Smith K C and Weaver J C 2005 Cylindrical cell membranes in uniform applied electric fields: validation of a transport lattice method *IEEE Trans. Biomed. Eng.* **52** 1643–53

[21] Pauly H and Schwan H P 1959 Über die Impedanz einer Suspension von Kugelförmigen Teilchen mit einer Schale *Z. Naturf.* B **14** 125–31

[22] Hanai T, Asami K and Koizumi N 1979 Dielectric theory of concentrated suspensions of shell-sphere in particular

reference to the analysis of biological cell suspensions *Bull. Inst. Chem. Res. Kyoto Univ.* **57** 297–305

[23] Mura T 1987 Micromechanics of defects in solids *Mechanics of Elastic and Inelastic Solids* 2nd edn (Dordrecht: Martinus Nijhoff)

[24] Bensoussan A, Lions J-L and Papanicolau G 1978 *Asymptotic Analysis for Periodic Structures* (Amsterdam: North-Holland)

[25] Sanchez-Palencia E 1980 *Non-Homogeneous Media and Vibration Theory (Lecture Notes in Physics)* (Berlin: Springer)

[26] Whittaker E T and Watson G N 1927 *A Course of Modern Analysis* (Cambridge: Cambridge University Press)

[27] Tricomi F 1951 *Funzioni Ellittiche* (Bologna: Nicola Zanichelli Editore)

[28] Apostol T M 1997 *Modular Functions and Dirichlet Series in Number Theory* 2nd edn (New York: Springer)

[29] Meguid S A and Kalamkarov A L 1994 Asymptotic homogenization of elastic composite with a regular structure *Int. J. Solids Struct.* **31** 303–16

[30] Rodríguez-Ramos R, Sabina F J, Guinovart-Díaz R and Bravo-Castillero J 2001 Closed-form expressions for the effective coefficients of a fiber-reinforced composite with transversely isotropic constituents: I. Elastic and square symmetry *Mech. Mater.* **33** 223–35

[31] Lord Rayleigh 1892 On the influence of obstacles arranged in rectangular order upon the properties of a medium *Phil. Mag.* **34** 481–502

[32] Nicorovici N A, McPhedran R C and Milton G W 1993 Transport properties of a three-phase composite material: the square array of coated cylinders *Proc. R. Soc. Lond.* A **442** 599–620

[33] Jiang C P, Xu Y L, Cheung Y K and Lo S H 2004 A rigorous analytical method for doubly periodic cylindrical inclusions under longitudinal shear and its applications *Mech. Mater.* **36** 225–37

[34] Parnell W J and Abrahams I D 2006 Dynamic homogenization in periodic fibre reinforced media: quasi-static limit for SH waves *Wave Motion* **43** 474–98

[35] Gu G and Liu Z 1992 Effects of contact resistance on thermal conductivity of composite media with a periodic structure *J. Phys. D: Appl. Phys.* **25** 249–55

[36] Cheng H and Torquato S 1997 Effective conductivity of periodic arrays of spheres with interfacial resistance *Proc. R. Soc. Lond.* A **453** 145–61

[37] Sangani A S and Mo G 1997 Elastic interactions in particulate composites with perfect as well as imperfect interfaces *J. Mech. Phys. Solids* **45** 2001–31

[38] Bigoni D, Serkov S K, Valentini M and Movchan A B 1998 Asymptotic models of dilute composites with imperfectly bonded inclusions *Int. J. Solids Struct.* **35** 3239–58

[39] Amar M, Andreucci D, Bisegna P and Gianni R 2006 On a hierarchy of models for electrical conduction in biological tissues *Math. Meth. Appl. Sci.* **29** 767–87

[40] Amar M, Andreucci D, Bisegna P and Gianni R 2004 Evolution and memory effects in the homogenization limit for electrical conduction in biological tissues *Math. Models Methods Appl. Sci.* **14** 1261–95

[41] Amar M, Andreucci D, Bisegna P and Gianni R 2007 Exponential asymptotic stability for an elliptic equation with memory arising in electrical conduction *Preprint 1* Department of Mathematical Models and Methods, University of Rome 'La Sapienza'

[42] Nicorovici N A, McKenzie D R and McPhedran R C 1995 Optical resonances of three-phase composites and anomalies in transmission *Opt. Commun.* **117** 151–69

[43] Perrins W T, McKenzie D R and McPhedran R C 1979 Transport properties of regular arrays of cylinders *Proc. R. Soc. Lond.* A **369** 207–25

[44] Roth B J, F L H Gielen and Wikswo J P 1988 Spatial and temporal frequency-dependent conductivities in volume-conduction calculations for skeletal muscle *Math. Biosci.* **88** 159–89

[45] COMSOL Inc. 2007 COMSOL Multiphysics™ User's Guide (version 3.4). http://www.comsol.com

[46] Zienkiewicz O C, Taylor R L and Zhu J Z 2005 *The Finite Element Method: Its Basis and Fundamentals* 6th edn (Amsterdam: Elsevier)

[47] Roth B J 2006 The electrical conductivity of tissues *The Biomedical Engineering Handbook* ed J D Bronzino, 3rd edn (Boca Raton, FL: Taylor and Francis) chapter 21

[48] Bradbury M G, Smye S W and Brocklebank J T 2001 Measurement of intercompartmental fluid shifts during haemodialysis in children *Physiol. Meas.* **22** 351–63